

A novel reentrant susceptibility due to vortex and magnetic dipole interaction in a $La_{1.85}Sr_{0.15}CuO_4$ and Gd_2O_3 composite system

Biswajit Dutta¹ and A. Banerjee²

¹*Ecole Normale Supérieure de Lyon, CNRS, Laboratoire de Physique, F-69342 Lyon, France*

²*UGC-DAE Consortium for Scientific Research, University Campus, Khandwa Road, Indore-452001, India.*

A reentrant behavior of temperature dependent magnetic ac-susceptibility (or excess susceptibility (ES)) at lower temperature is observed in a composite made of superconductor $La_{1.85}Sr_{0.15}CuO_4$ (LCu) and an insulating paramagnetic salt Gd_2O_3 (GdO). The ES exhibits an exponential characteristic that varies with temperature ($\exp, [-\frac{T_0}{T}]$), T_0 is characteristics temperature. The characteristics temperature, T_0 , decreases as the effective interface diminishes and the amplitude of the dc magnetic field increases. The creation of ferromagnetic dimers between Gd^{+3} ions in GdO is observed as a result of vortex-dipole interaction, which causes the observation of this unusual ES at temperatures much lower than the superconducting onset temperature T_S^{onset} . This type of ferromagnetic dimer formation much below superconducting transition temperature is found comparable with the formation of Yu-Shiba-Rusinov (YSR) state and interaction between these YSR state.

PACS numbers: 75.47.Lx, 71.27.+a, 75.40.Cx, 75.60.-d

I. INTRODUCTION

A coherent many-body state of electron pairs with zero spin forms in many materials, leading to the emergence of superconducting (SC) order. This state is associated with an energy gap, which represents the energy required to break a pair by adding or removing an electron, leaving an unpaired electron [1]. In most materials, interactions that promote magnetism tend to undermine the superconducting order. Local superconducting order depletion can occur when magnetic contaminants are present, and one of the consequence of presence of magnetic contaminants is the emergence of an in-gap bound states known as Yu-Shiba-Rusinov (YSR) states [1–9].

The YSR state has been discovered at the edges of a ferromagnet and a superconducting hybrid system [2–5]. The localized magnetic moment combines with the superconductor's anti-aligned spin state to create the YSR state, which has discrete spin polarization and an energy E_b that is less than the size of the superconducting energy gap Δ (i.e., $E_b < \Delta$). This state facilitates a spin triplet ground state [2], and the wave function of this YSR state has a spatially oscillatory, decaying structure [6–9].

When two parallel-spin impurities pair, the hybridization of these YSR states (due to the overlap of the wave functions) results in Shiba bands in these structures [10,11]. Experimental work has focused on examining the Shiba states of single magnetic impurities on superconducting substrates and of coupled dimers of such impurities, with the goal of tailoring the Shiba bands for topological superconductivity [10–19].

Interestingly, an excess susceptibility (ES) or upturn in the susceptibility has been previously reported in a composite system of the superconductor niobium (Nb) with the normal metals silver (Ag) or gold (Au) [20, 21, 23, 24]. This behavior was initially explained in terms of the formation of a "p-wave" superconducting bound state in

the novel metal, due to the proximity of the superconductor. However, the precise cause of this anomalous ES or upturn remains to be unambiguously identified.

Notably, the theoretical work of Roman M. Lutchyn et al. has modeled that the interface between an 's-wave' superconductor and a material with strong spin-orbit coupling, such as the novel metals Ag and Au, can provide a fertile ground for the appearance of Majorana Zero modes [25]. Furthermore, the zero-energy excitation of the 'Shiba' band is also found to carry information about the topological superconductor and the Majorana modes [2, 4, 13].

These proximity-induced effects in hybrid superconducting systems warrant further scrutiny to fully understand the underlying mechanisms behind the observed anomalous magnetic susceptibility behavior. The interplay between superconductivity, magnetism, and spin-orbit coupling at these interfaces presents an intriguing avenue for exploring exotic quantum phenomena and potentially realizing topological superconductivity.

In this work, we report an anomalous excess susceptibility (ES) at very low temperatures in composites of the superconductor $La_{1.85}Sr_{0.15}CuO_4$ (LCu) and the paramagnetic material Gd_2O_3 (GdO), which has a large spin magnetic moment of approximately $7\mu_b$. The ES is influenced by changes in the interface between GdO and LCu, and by the application of a dc magnetic field that destroys superconductivity. This ES is similar to phenomena observed in Nb and Au/Ag composite systems.

We observed a finite value of the second-order susceptibility ($|\chi_2|$) even in the absence of a DC magnetic field. The increased susceptibility at low temperatures, along with a nonzero second-order susceptibility ($|\chi_2|(T)$) at zero-bias DC field, indicates a modulated ferromagnetic or ferrimagnetic interaction between Gd^{+3} spins. The modulation induced by the DC magnetic field suggests that this interaction is mediated through vortices, implying a signature of vortex and magnetic dipole interaction. The scaling of the excess susceptibility with the effective

interface between GdO and LCu, along with the magnetic field, suggests the opening of an energy gap with an amplitude smaller than the superconducting energy gap. This phenomenon is further elaborated in the experimental results section. Additionally, these observations indicate the emergence of a spin triplet Yu-Shiba-Rusinov (YSR) type dimer state.

To modify the effective interface, we prepared two sets of composites. In the first set, we maintained fixed particle sizes but varied the weight percentages of LCu and GdO. In the second set, we kept the LCu particle size and the weight percentages of LCu and GdO constant, while varying the particle size of GdO. We employed both linear and nonlinear AC susceptibility measurement techniques to study these composites.

It is noteworthy that linear and nonlinear AC susceptibility measurements are crucial tools for characterizing various properties of type-II superconductors, including determining critical thermodynamical parameters such as critical current, critical field, and critical temperature [26–29]. Moreover, these techniques are highly effective in distinctly identifying various metastable states such as spin-glass, cluster glass, and superparamagnet [30–36], as well as in studying long-range ordered systems like ferromagnets, ferrimagnets, and antiferromagnets [37–39].

II. EXPERIMENTAL DETAILS

A. Sample preparation and characterization

$La_{1.85}Sr_{0.15}CuO_4$ (LCu) sample is prepared by pyrophoric method [40] and final heat treatment is done at 950°C . Then LCu and commercial Gd_2O_3 (GdO) powder of 99.99% purity are mixed in three different weight ratios and grind them very carefully to mix uniformly. Then the mixed powder is palletized at considerable high pressure ~ 150 kN and heated at 830°C for 4 hrs to prepare the composite. The three composite thus made have the weight percentage and nomenclature as follows:

LCu (94%)+GdO(6%)-B1,
 LCu (90%)+GdO(10%)-B2,
 LCu (76%)+GdO(24%)-B3,

To make the second set of three composites, nanoparticles of GdO is prepared by pyrophoric method. Then the precursor powder obtained from pyrophoric method is heated at three different temperatures, like 600°C , 800°C and 950°C to vary the particle size of GdO. Then the precursor powder of LCu and GdO (different particle sizes) are mixed in 90:10 weight ratio (i.e., 90 weight percentage of LCu and 10 weight percent of GdO) and heated at 550°C to prepare the composites whose details and attributed nomenclature is given

LCu (90%)+GdO600(10%)-B4,
 LCu (90%)+GdO800(10%)-B5,
 LCu (90%)+GdO950(10%)-B6

The samples are characterized by X-ray diffraction (XRD) performed in Bruker X-ray diffractometer from

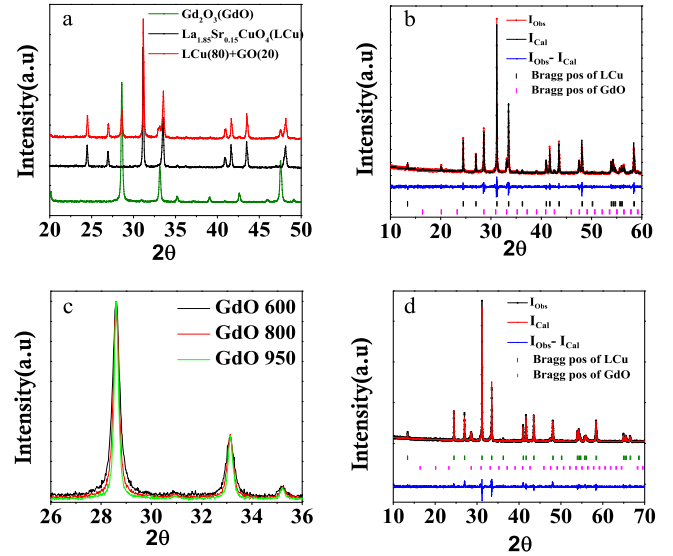


FIG. 1. (Colour Online)(a) Room temperature XRD pattern of composites B3 and the parent the ingredients LCu and GdO respectively. (b) Rietveld refinement of the composite B3(LCu (76%)+GdO(24%)). (c) XRD pattern of GdO heated at various temperature. (d) Rietveld refinement of the composite B2(LCu (90%)+GdO600(10%)).

TABLE I. Best fitted parameters, PS- particle size, SG- space group, PF- phase fraction

Mateial	PS(nm)	SG	a=b(\AA)	c(\AA)	PF	R_f
(LCu)	bulk	I4/mmm	3.777(2)	13.222(9)	NA	1.35
(GdO)	bulk	I213	10.818(4)	10.818(4)	NA	1.44
(GdO600)	25	I213	10.820(4)	10.820(4)	NA	1.44
(GdO800)	45	I213	10.815(4)	10.815(4)	NA	1.44
(GdO950)	60	I213	10.813(4)	10.813(4)	NA	1.44
B1(LCu)	bulk	I4/mmm	3.779(1)	13.223(9)	96	1.47
B1(GdO)	bulk	I213	10.819(6)	10.819(6)	4	1.47
B2(LCu)	bulk	I4/mmm	3.777(1)	13.220(9)	96	1.47
B2(GdO)	bulk	I213	10.819(6)	10.816(6)	4	1.47
B3/(LCu)	bulk	I4/mmm	3.779(4)	13.226(6)	76	1.44
B3/(GdO)	bulk	I213	10.817(6)	10.817(6)	24	1.44
B4/(LCu)	bulk	I4/mmm	3.782(3)	13.223(1)	91	1.8
B4/(GdO600)	25	I213	10.816(8)	10.816(3)	9	1.8
B5/(LCu)	bulk	I4/mmm	3.784(1)	13.228(8)	92	1.6
B5/(GdO800)	45	I213	10.814(9)	10.814(1)	8	1.6
B6/(LCu)	bulk	I4/mmm	3.784(5)	13.227(7)	92	1.87
B6/(GdO950)	60	I213	10.812(1)	10.812(7)	8	1.87

$10^\circ - 90^\circ$ at an interval of 0.02° . Fig. 1a shows representative XRD patterns of the parent paramagnet (GdO) and superconductor (LCu) along with the two phase Rietveld refinement of the composites. Fig.1b shows the two phase Rietveld refinement of XRD data of the composite B3. Fig. 1c shows the XRD pattern of GdO annealed at various temperatures resulting in different particle sizes exemplified by the difference in full width at half maxima (FWHM). Particle sizes obtained from the Williamson

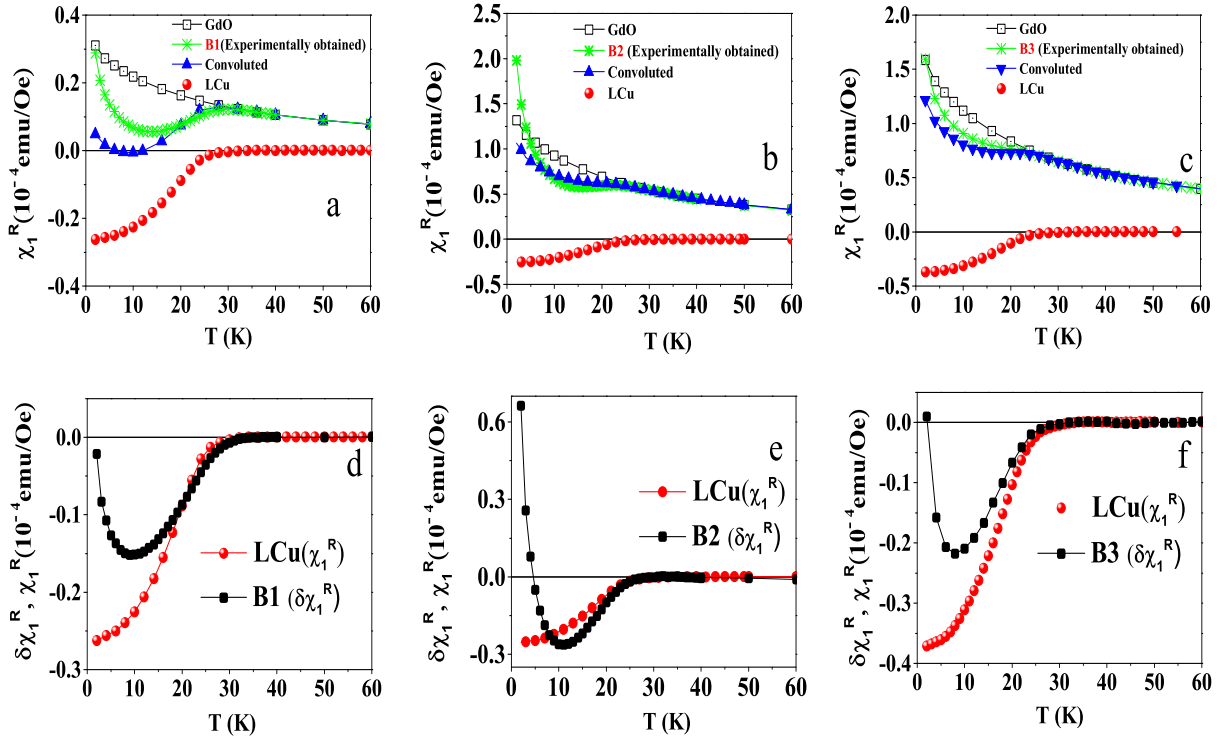


FIG. 2. (Colour Online) (Colour Online) Ac-susceptibility measurements are performed in an ac-field of 3 Oe and frequency 231.1 Hz, (a) Comparative plot of the real part of first order ac-susceptibility (χ_1^R) against temperature of the composite B1, LCu, GdO and linear superimposed (or the simple convoluted) χ_1^R . Similar type of plot for the composite B2 and B3 is shown in (b) and (c), respectively. The temperature dependent deconvoluted susceptibility ($\delta\chi_1^R$) plot for B1, B2 and B3 is shown in (d), (e) and (f), respectively, along with them the normalized susceptibility plot (χ_1^R) of LCu is also plotted with each deconvoluted graph.

Hall Plot are 25 nm, 45 nm and 60 nm for samples annealed at 600°C, 800°C and 950°C respectively. Fig.1d shows the two phase Rietveld refinement of XRD data of the composite B2 i.e. LCu (90%)+GdO600(10%).

From the XRD pattern and the Rietveld refinement of the composite no impurity phase could be identified confirming no chemical reaction taken place between the ingredients LCu and GdO. The lattice parameters of LCu and GdO obtained from the two phase Rietveld refinement of all the composites depicts no significant change with respect to the corresponding raw materials i.e. LCu and GdO.

The value of the lattice parameters of the corresponding raw materials and the ingredients present in all the composites are provided in Table I. No significant change in the lattice parameters of the ingredients in the composites with respect to their parent or raw material indicates that there is no considerable lattice strain is developed in either ingredients while preparing the composites. The details of space group (SG), lattice parameters, phase fraction (PF), particle size(PS) etc. are listed in Table I. The PFs obtained from two phase Rietveld refinement are used to calculate the amount of GdO and LCu present in the composite per unit gram (gm) which is used to

normalize the ac-susceptibility value of the composite.

B. Magnetic measurements

The Low field linear and nonlinear magnetic ac-susceptibility measurements have been performed using a homemade ac-susceptometer, which can be operated down to 4.2K from 300K and the measurements can be done in both cooling and heating cycle with a temperature accuracy of 1mK. The estimated sensitivity of the setup is $\sim 10^{-7}$ emu [41]. The higher dc-field (> 200 Oe) superimposed ac-susceptibility measurements are performed in MPMS-XL (M/S, Quantum Design). Low field ac-susceptibility measurement probes the spin dynamic at very low field. The magnetization (m) can be expanded with respect to the applied ac-field h_{ac} as

$$m = m_0 + \chi_1 h + \chi_2 h^2 + \chi_3 h^3 + \chi_4 h^4 \dots (1)$$

$\chi_1 (\approx \delta m / \delta h)$ is linear susceptibility and $\chi_2, \chi_3, \chi_4 \dots$ are nonlinear susceptibilities. These nonlinear susceptibilities contain many fruitful information but magnitude of these

are much smaller (couple of order) than the linear susceptibility, therefore they are difficult to measure from normal dc-magnetization measurement, but these nonlinear susceptibilities can be easily measured from high sensitive ac-susceptibility measurement [32, 35, 41]. If the magnetization has an inversion symmetry with respect to the applied ac-field (h_{ac}) then all the even order susceptibilities, like $\chi_2(\approx \delta^2 m / \delta^2 h)$, $\chi_4(\approx \delta^4 m / \delta^4 h)$ do not appear in the absence of external dc-field (at $h_{dc} = 0$ Oe) like paramagnetic and antiferromagnetic materials, but when the inversion symmetry breaks by internal field then $\chi_2, \chi_4..$ all the even order susceptibility shows finite value (at $h_{dc} = 0$ Oe), like in case of ferromagnet, or ferrimagnetic state [42, 43]. Even order susceptibilities also appear when external dc-field is applied, superimposing on ac-field. The third order susceptibility (χ_3) is very useful tool to unambiguously distinguish various metastable states like spin glass (SG), superparamagnet (SPM) etc. [30–36]. χ_3 is also found as very effective tool in determining the universality class of the ferromagnet i.e. to study the nature of magnetic ground state of the corresponding ferromagnet [37–39].

III. RESULTS AND DISCUSSIONS

The combined temperature-dependent plot of χ_1 (the real component of the first-order AC susceptibility), $\chi_1^R(T)$, for the composites B1, B2, and B3 is presented in FIG. 2. This plot is accompanied by the $\chi_1^R(T)$ plot of the parent constituents LCu and GdO for comparative purposes. To demonstrate the proximity effect resulting from the interaction between LCu and GdO, the mass-normalized convoluted and deconvoluted components are also included in these graphs. The $\chi_1^R(T)$ plots for the composites (B1, B2, B3 - Green stars), LCu (Red circles), and GdO (Black squares), as well as the convoluted susceptibility of LCu and GdO (Blue triangles), are displayed in FIG. 2a, FIG. 2b and FIG. 2c, respectively.

Convolution is performed by combining the mass-normalized susceptibility data of the parent materials, LCu and GdO. The susceptibility graph of parent GdO is normalized relative to the mass of GdO present in the composite used for susceptibility measurement. Similarly, the susceptibility graph of LCu is normalized relative to the mass of LCu present in the composite. In FIG. 2a, FIG. 2b and FIG. 2c, all graphs converge above the onset temperature of superconductivity ($T_S^{(onset)}$). These observations indicate that the magnetization value (spin moment only, as $L = 0$ for Gd^{+3} ion) of the mole-normalized GdO present in the composite and the parent GdO (mole-normalized) are equivalent. This suggests that there was no chemical reaction between the LCu and GdO components during the composite preparation.

Since LCu is a Pauli paramagnetic substance, its temperature-dependent susceptibility should be temperature-independent and very small in magnitude above $T_S^{(onset)}$ compared to GdO. Thus, it should not

affect the Curie-Weiss susceptibility behavior of GdO above $T_S^{(onset)}$ [43]. The amplitude of the experimentally measured susceptibility values of the composites (Green stars) shows a greater magnitude than the convoluted data (Blue triangles) at much lower temperatures (approximately 7 to 9 K), where GdO starts deviating from Curie-Weiss behavior, as shown in FIG. 2a, FIG. 2b and FIG. 2c. Therefore, this additional susceptibility appears to result from either a reduction in the diamagnetic portion of LCu or the emergence of a specific type of modulated magnetic interaction at the bulk and interface of LCu and GdO.

The diamagnetic fraction of LCu can change for several reasons, including: 1-Alteration of LCu's crystal structure and crystalline size during composite preparation. 2-Chemical reaction between LCu and GdO, which can also destroy superconducting properties. 3-Pinning of vortices due to magnetic interaction between LCu and GdO across the interface. XRD measurements show no significant change in the crystal structure of LCu and GdO during composite preparation and depict the absence of extra impurity peaks other than those of LCu and GdO. Additionally, the same value of μ_{eff} for the composites and GdO (calculated from Curie-Weiss fitting of the $\chi_1^R(T)$ graph above $T_S^{(onset)}$) eliminates the possibilities mentioned in points (1) and (2). The remaining possibility is the interaction between GdO and LCu across the interface, which alters the magnetic properties of the composite relative to the convoluted data.

To better visualize the changes in magnetic properties due to the mutual interaction between LCu and GdO, a deconvolution operation was performed. Specifically, we subtracted the mass-normalized susceptibility data of GdO from the susceptibility data of the composite. This deconvoluted susceptibility, normalized by the same previously mentioned mass value, is denoted as $\delta\chi_1^R$. The resulting temperature-dependent deconvoluted susceptibility, $\delta\chi_1^R(T)$, is plotted alongside the mass-normalized susceptibility, $\chi_1^R(T)$, of LCu. These combined plots are presented in FIG. 2d, FIG. 2e, and FIG. 2f for samples B1, B2, and B3, respectively.

It is noteworthy that there is no discernible difference between the values of $\delta\chi_1^R(T)$ and $\chi_1^R(T)$ for LCu around the onset temperature, $T_S^{(onset)}$. This indicates that the chemical composition of LCu in the composite remains unchanged from that of the parent LCu. However, a sudden change in $\delta\chi_1^R(T)$ below 10 K ($\sim -10^{-5}$ emu to $+10^{-5}$ emu) suggests that the interaction extends beyond the surface or interface, penetrating into the bulk of one of the components.

In the $\delta\chi_1^R(T)$ plot for B1, a minimum is observed at 7 K, followed by an upturn below this temperature. This behavior is absent in the parent LCu, which does not exhibit any anomalies in this temperature range. The composite B2, as shown in FIG. 2e, exhibits the most significant anomaly in low-temperature $\delta\chi_1^R(T)$ among all the composites. Although the onset temperature, $T_S^{(onset)}$,

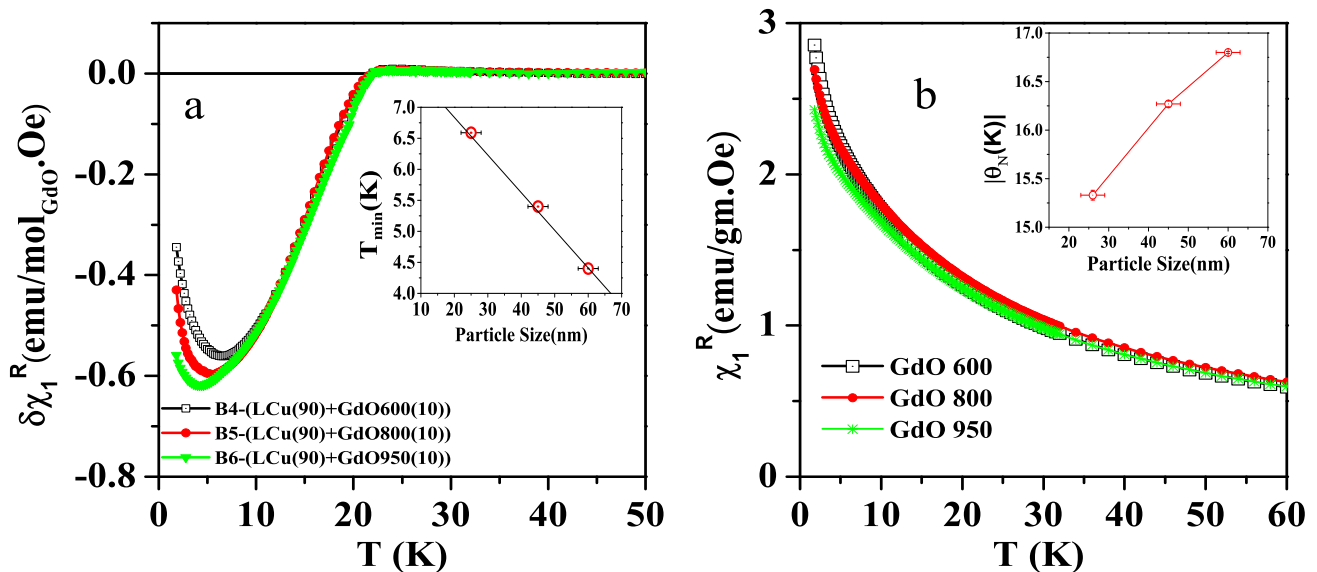


FIG. 3. (Colour Online) All the measurements has been performed in an ac field of 3 Oe and frequency 231.1 Hz (a) Normalized $\delta\chi_1^R$ against temperature for B4, B5 and B6 composite respectively. Inset shows the plot of T_{min} against the particle size of GdO and the red line corresponds to the straight line fitting. (b) Normalized χ_1^R is plotted against temperature for GdO600, GdO800 and GdO950 respectively (Inset shows the plot of Curie-Weiss temperature (θ_N) against the particle size of GdO).

TABLE II. Best fitted parameters

Composite	T_{min} (K)	Paricle size of GdO(nm)	$ \theta_N $ (K)	C_{cal} (emu/mole.K)
B4	6.60	25	15.3 ± 0.08	8.07 ± 0.05
B5	5.40	45	16.2 ± 0.04	7.90 ± 0.07
B6	4.40	60	16.8 ± 0.02	7.98 ± 0.05

remains constant across all composites, the minimum value of $\delta\chi_1^R(T)$ is observed at different temperatures: 7 K for B1, 11 K for B2, and 8 K for B3. This variability suggests that the anomalous excess susceptibility is an interface-induced phenomenon resulting from the magnetic interaction between GdO and LCu.

The interface effect is further corroborated by modulating the effective interface between LCu and GdO through varying the GdO particle size while maintaining a constant mass ratio. Herein, we present the results corresponding to the composition (mass ratio) of composite B2 (i.e., LCu(90) + GdO(10)). The effective interface between LCu and GdO is altered with changes in particle size due to the resultant modifications in the surface-to-volume ratio of GdO. The plot of $\delta\chi_1^R(T)$ for the composite containing GdO600, GdO800, and GdO950 (denoted as B4, B5, and B6, respectively) is illustrated in FIG. 3a. The values of $\delta\chi_1^R(T)$ for all these composites are calculated similarly to the method described previously. The results indicate that $T_S^{(onset)}$ remains constant across all composites (i.e., B4, B5, and B6). Additionally, the unchanged values of orthorhombic distortion suggest no variation in the hole concentration of LCu, implying the chemical state of LCu in all composites remains consistent.

However, a progressive decrease in T_{min} with increasing GdO particle size (i.e., for B4, T_{min} is observed at approximately 6.6 K, and for B6, it is observed around 4.4 K) suggests that the low-temperature anomaly or the existence of electronic scattering (ES) is an interface-induced phenomenon. The specifics of the GdO particle size in composites B4, B5, and B6, along with the Curie-Weiss temperature (θ_N (K)), Curie-Weiss constant (C), and T_{min} (K) values, are provided in Table II. The inset of FIG. 3a depicts the variation of T_{min} with GdO particle size, demonstrating that the interaction between LCu and GdO becomes more pronounced as the GdO particle size decreases.

The effects of particle size reduction include:

Enhanced interaction efficiency between LCu and GdO. As shown in FIG. 3b, the susceptibility value of GdO increases at lower temperatures. The Neel temperature (θ_N) of GdO also decreases, as illustrated in the inset of FIG. 3b. The first result has been previously described, while the second and third observations indicate that the antiferromagnetic (AFM) correlation between the Gd^{+3} spins diminishes with decreasing GdO particle size. This leads to an increase in the number of unpaired Gd^{+3} spins on the surface and within the bulk of GdO [44–46]. Due to the heightened interaction probability

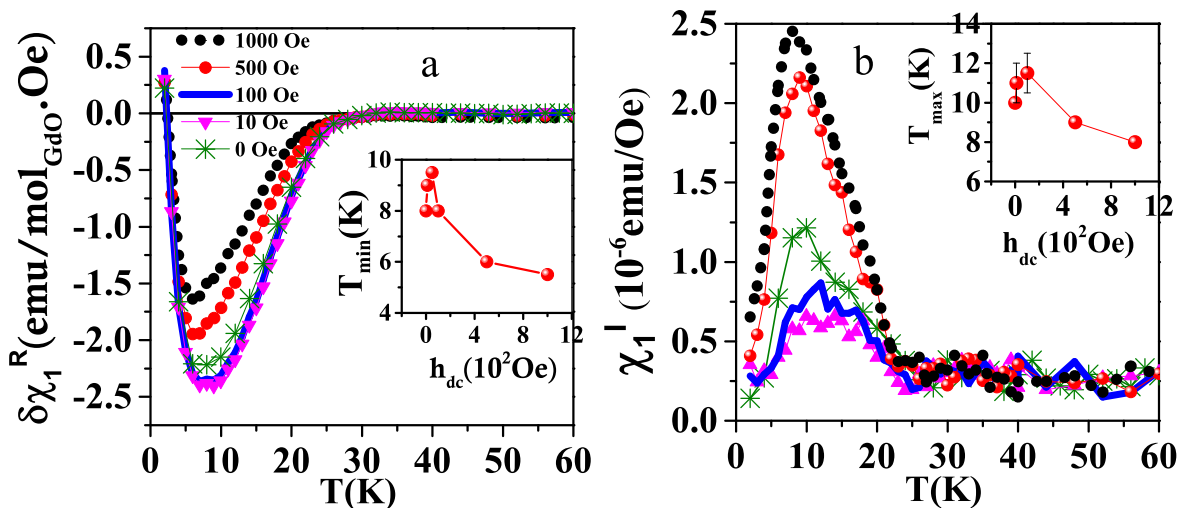


FIG. 4. (Colour Online) All the measurements are done in an ac field of 3 Oe and frequency 231.1 Hz in B3 composite (a) $\delta\chi_1^R$ is plotted against temperature in superimposed dc field of amplitude 0, 10, 100, 500 and 1000 Oe respectively, (Inset shows dc field dependent plot of T_{min}). (b) χ_1^I is plotted against temperature for various amplitude of dc fields (0, 10, 100, 500 and 1000 Oe). Inset shows the dc field dependent plot of T_{max} .

between GdO and LCu and the larger effective interface, composite B4 exhibits the most significant $\delta\chi_1^R$ anomaly at lower temperatures compared to B5 and B6.

An important observation is that the upturn in $\delta\chi_1^R$ (depicted in FIG. 3a) is not as sharp as in the $\delta\chi_1^R(T)$ graphs of B1, B2, and B3 (shown in FIG. 2d, FIG. 2e, and FIG. 2f). This difference is attributed to the annealing temperatures: B1, B2, and B3 composites are annealed at a higher temperature (830°C), whereas B4, B5, and B6 are annealed at a comparatively lower temperature (550°C). This results in lower compactness (or intergranular contact) in B4, B5, and B6 compared to B1, B2, and B3. The linear decrease in T_{min} and the gradual suppression of $\delta\chi_1^R(T)$ below T_{min} with increasing GdO particle size (as shown in the inset of FIG. 3a) imply that the low-temperature upturn in the $\delta\chi_1^R(T)$ graph is an intrinsic mesoscopic effect of the LCu and GdO proximity structure.

To gain a deeper understanding of the observed anomaly, we propose a model wherein the unpaired Gd^{+3} spins interact with vortices via vortex dipole interactions. Given the substantial magnetic moment of the Gd^{+3} spin ($7\mu_B$), it can generate significant local magnetic fields and effectively couple with the vortices within the superconductor. To further investigate this interaction, we conducted dc-field superimposed ac-susceptibility measurements.

The primary function of the applied dc magnetic field is to modulate the vortex dipole interactions. This modulation occurs through the induction of the Lorentz force on the vortices and the Zeeman interaction, which biases the uncompensated Gd^{+3} spins in GdO. The resultant $\delta\chi_1^R(T)$ graph is expected to reflect these phenomena. Specifically, the $\delta\chi_1^R(T)$ graph at various superimposed dc-fields is depicted in FIG. 4a (for the B3 composite).

The experimental procedure is as follows:

Measurement: Initial dc-field superimposed ac-susceptibility measurements were performed on each parent component and composite. Data Extraction: Subsequently, a deconvolution method was employed to determine the $\delta\chi_1^R(T)$ values for each dc-field, consistent with the methodology discussed in the preceding section. As illustrated in FIG. 4a, the diamagnetic fraction and T_{min} of $\delta\chi_1^R(T)$ increase for lower dc bias fields ($h_{dc} < 100$ Oe) compared to the $\delta\chi_1^R(T)$ at $h_{dc} = 0$ Oe. However, for dc bias fields exceeding 100 Oe, both the diamagnetic fraction and T_{min} decrease. The inset of FIG. 4a shows the trend of T_{min} versus the superimposed dc-field, indicating an initial increase in T_{min} up to 100 Oe of dc-field, followed by a subsequent decrease above 100 Oe. This behavior underscores the complex interplay between the magnetic field, vortex dynamics, and Gd^{+3} spins in the composite.

In FIG. 4b, the temperature-dependent imaginary component of the linear susceptibility under an applied dc-field ($\chi_1^I(T)$) is depicted. The plot reveals an initial minor increase in the peak temperature (T_{max}) up to 100 Oe of dc-field. Notably, the peaks of the graph for the dc-fields of 10 Oe and 100 Oe exhibit minimal variation, thus for these cases, the midpoint was taken as T_{max} , with corresponding error bars added to these data points, as illustrated in the inset of FIG. 4b. Additionally, a decrease in the amplitude of the loss component is observed. Beyond 100 Oe, or at higher dc-field amplitudes, T_{max} decreases steadily, as indicated in the inset of FIG. 4b, while the peak height of χ_1^I increases correspondingly.

According to the Bean model [26], the loss peak corresponds to the temperature at which the magnetic field penetrates the center of the superconducting specimen

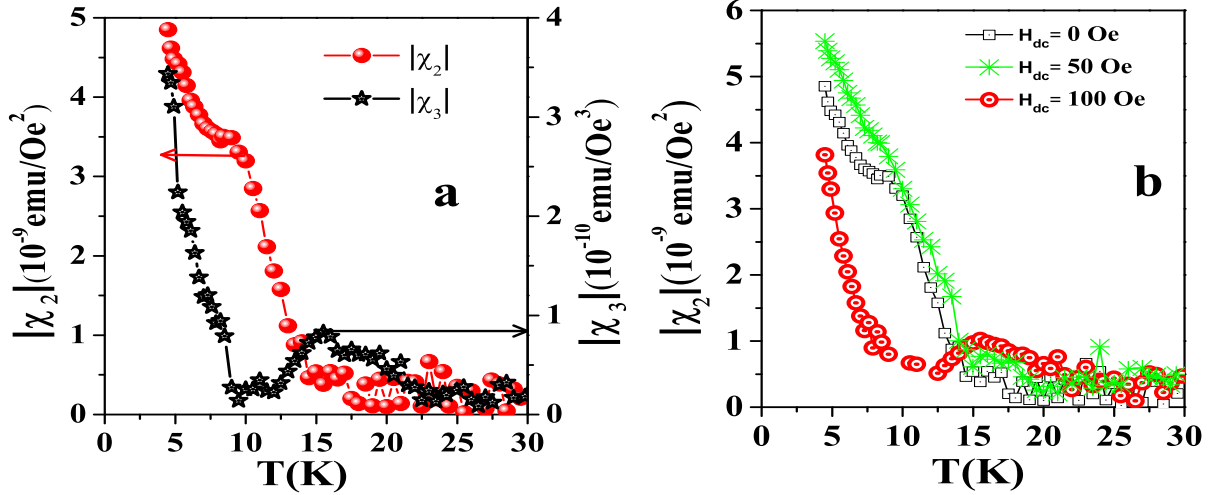


FIG. 5. (Colour Online) second order ac susceptibility ($|\chi_2|$) is plotted against temperature (Left hand side Y axis is the corresponding scale) and Third order ac susceptibility ($|\chi_3|$) is plotted against temperature (Right hand side Y axis is the corresponding scale) for composite B3. (b) $|\chi_2|$ against temperature in three superimposed dc field (0 Oe, 50 Oe and 100 Oe) for composite B3.

or the point at which the critical current density (J_C) of the superconductor diverges. At low dc-field amplitudes, the GdO component remains in a paramagnetic state, exhibiting no anomalies in the $\chi_1^I(T)$ graph within this temperature range. However, at higher dc-field amplitudes, the spins of the paramagnetic component tend to align with the dc-field, resulting in a reduced response to the applied ac-field. Consequently, a loss component or a finite value of $\chi_1^I(T)$ is observed in the ac-susceptibility measurement.

The observed decrease in the loss peak height up to a dc-field of 100 Oe is accompanied by a slight increase in the critical current density of B3. Consequently, a modest increase in T_{max} (~ 1 ,K) is noted. As the critical current density decreases beyond this field, the loss peak shifts toward lower temperatures. The unpaired spins of GdO may contribute to the rise in the magnitude of χ_1^I . This effect arises because, as previously indicated, these spins become biased under the influence of the higher dc bias field and do not respond to the applied ac-field, thereby increasing the amplitude of χ_1^I .

The vortex dipole interaction model can also explain the dc-field dependent behavior of T_{min} and T_{max} . Given that Gd^{+3} ions possess a large spin magnetic moment ($\sim 7\mu_b$) even a small magnetic field can exert significant torque on them. At low temperatures, where the thermal fluctuation of Gd^{+3} spins is suppressed, the interaction probability increases. When a dc-field is applied in this context, the thermal fluctuation of Gd^{+3} spins reduces further at lower dc bias field values. Since the dc-field lacks sufficient energy to mobilize the vortices owing to its smaller amplitude, the interaction probability between the vortex and the magnetic dipole increases. This interaction enhances the vortex pinning strength, resulting in an increased amplitude of the critical cur-

rent density, which in turn leads to an increase in and a decrease in the peak height of χ_1^I .

Additionally, the increase in critical current density leads to a rise in the diamagnetic fraction of $\delta\chi_1^R(T)$ and T_{min} within the dc-field range of 0-100 Oe. However, as the dc bias field exceeds 100 Oe, the Lorentz force becomes strong enough to mobilize the vortices. This mobilization results in finite vortex motion, reducing the interaction probability between the vortex and the dipole. Consequently, T_{max} of χ_1^I shifts to a lower temperature, along with T_{min} of $\delta\chi_1^R$ and the diamagnetic fraction of $\delta\chi_1^R(T)$ also decreases. Here the picture we want to convey is like, In type II superconductors, the interaction between vortices can mediate an indirect coupling between Gd^{+3} spins. This vortex-mediated interaction leads to a ferromagnetic or ferrimagnetic ordering of the Gd^{+3} spins. This dc-field dependent behavior clearly indicates that the anomalous electromagnetic shielding (ES) is predominantly due to the vortex-dipole interaction. Moreover, it is significant to note that the ES value at lower temperatures is relatively high (approximately $\sim 10^{-5}$ emu), suggesting that this phenomenon extends beyond the interface and impacts the bulk material as well. If the argument regarding excess susceptibility presented above is correct, then an internal field should have developed as a result of this ferrimagnetic (or ferromagnetic) type of modulated spin arrangement. This internal field should have been visible in the χ_2 (second-order susceptibility) measurement without a superimposed DC field, and it can also be tuned by adjusting the vortex-dipole interaction (or by changing the DC field amplitude). The temperature-dependent plot of the second-order AC susceptibility for the composite B3 is shown in FIG. 5a without a superimposed DC field ($|\chi_2|$, left-hand side Y-axis scale). It demonstrates that the anomaly in $|\chi_2|$ appears

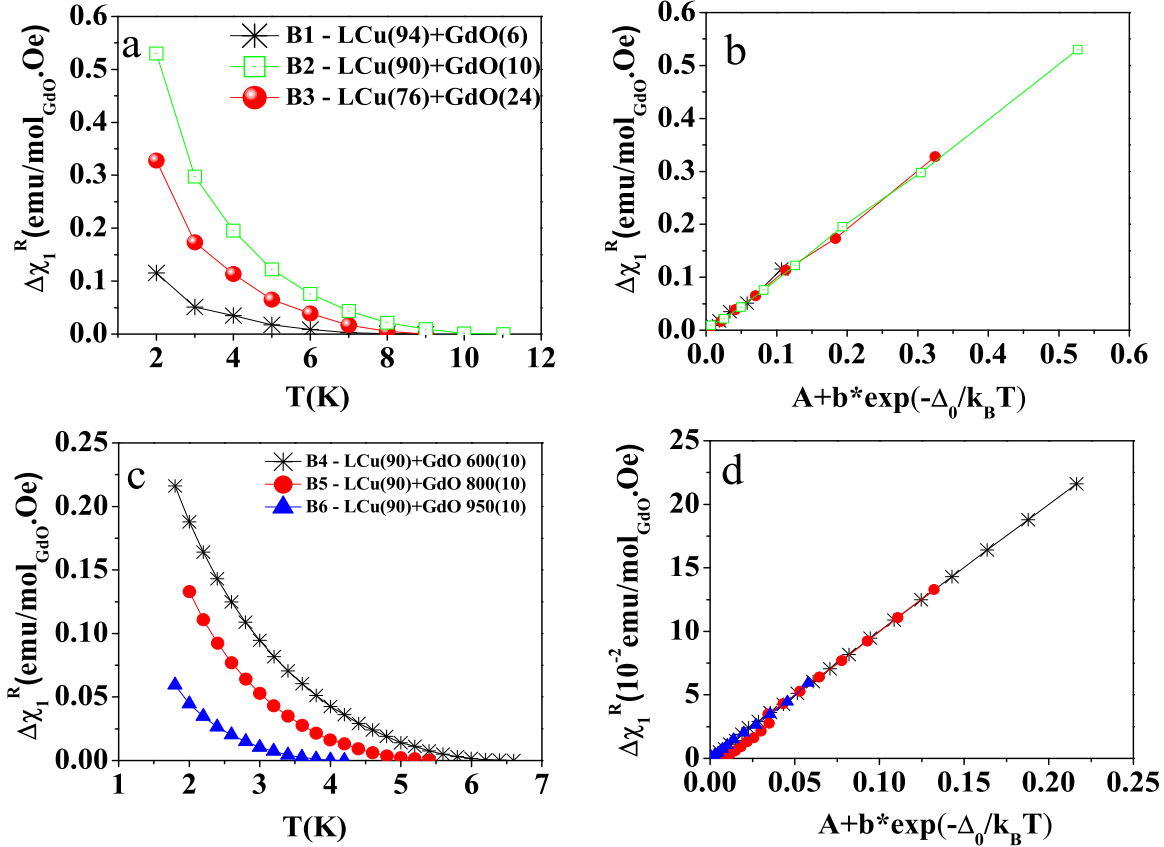


FIG. 6. (Colour Online)(a) $\Delta\chi_1^R$ is plotted against temperature for the composite B1, B2 and B3. (b) $\Delta\chi_1^R$ is plotted against scaled temperature axis. (c) $\Delta\chi_1^R$ is plotted against temperature for the composite B4, B5 and B6. (d) $\Delta\chi_1^R$ is plotted against scaled temperature axis.

below 15 K and a second anomaly is observed below 10 K, where $|\chi_2|$ exhibits an almost divergent behavior. In any magnetic substance, $|\chi_2|$ appears in the presence of a symmetry-breaking field [36, 39, 42]. The anomaly of $|\chi_2|$ below 15 K in zero DC field thus confirms that the ordering nature of the Gd^{+3} spins is of the ferromagnetic (or ferrimagnetic) kind and is a signature of some kind of internal symmetry-breaking field.

Similar measurements were conducted for the parent compounds GdO and LCu. Because GdO is a paramagnetic material and exhibits a paramagnetic to anti-ferromagnetic (AFM) transition below 3 K, there is no anomaly in $|\chi_2|$ with zero superimposed DC field [44–46]. Since AFM has no internal field, $|\chi_2|$ remains zero down to the lowest measurable temperature. In the case of LCu, $|\chi_2|$ appears only in the presence of a superimposed DC field with the AC field or when the critical current density becomes a function of the applied DC field [27–29]. The temperature-dependent plot of $|\chi_2|$ at three superimposed DC fields (0, 50, and 100 Oe) is shown in FIG. 5b. It demonstrates that as the DC field amplitude increases, $|\chi_2|$ initially increases (up to 50 Oe) and then decreases at higher values of the DC field (at

and above 100 Oe). These results reveal that the internal field amplitude increases up to a particular DC bias field value and decreases at higher DC field values, indicating a tunable behavior.

The modulated ferromagnetic (or ferrimagnetic) type interaction between Gd^{+3} ions is therefore described by the DC field-dependent graph of $|\chi_2|$ and follows a similar DC field-dependent behavior as found in the case of T_{min} , T_{max} , $\chi_1^I(T)$, and $\delta\chi_1^R(T)$ (discussed previously). This description is also supported by the size effect analysis of GdO (FIG. 3a), where it is seen that the proximity effect-induced ferromagnetic type of modulation between Gd^{+3} spins increases as the AFM ordering tendency between the Gd^{+3} spins decreases (i.e., with decreasing particle size shown in FIG. 3b). This is why, as shown in FIG. 3a, the low-temperature excess susceptibility in the $\delta\chi_1^R(T)$ graph and T_{min} is observed at a higher temperature in the case of B4 compared to B5 and B6.

The temperature-dependent graph of third-order susceptibility ($|\chi_3|(T)$) is also shown in FIG. 5a (right-hand side Y-axis scale). It shows two anomalies: one at high temperature (25 K - 12 K) and another at low temperature (below 12 K). Generally, χ_3 appears due to the

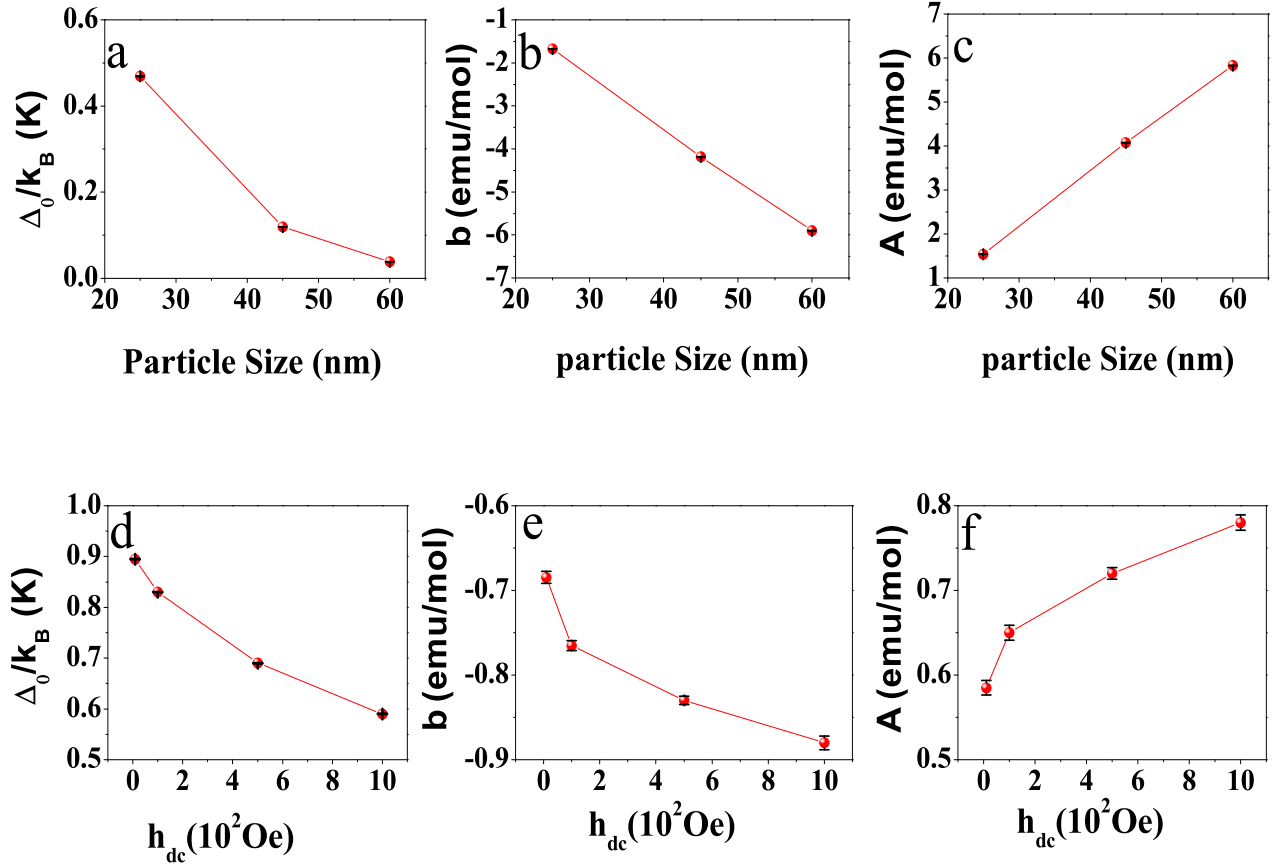


FIG. 7. (Colour Online)(a) T_0 is plotted against the particle size.(b) Parameter "b" is plotted against the particle size.(c) Parameter "A" is plotted against the particle size.(d) The exponential fitting of dc field superimposed susceptibility graph of composite B3.(e) and (f) shows the dc field dependent plot of T_0 and b. Inset shows the dc field dependent plot of parameter A.

irreversibility of flux motion in a superconductor [26]. The high-temperature anomaly is due to irreversibility in flux motion inside the grain, and the lower temperature anomaly (below 10 K) might be associated with the modulated ordering of Gd^{+3} spins. Therefore, the fundamental susceptibility graph and the higher-order susceptibility graph represent the low-temperature anomalous excess susceptibility, which is a result of the magnetic interaction between Gd^{+3} spins being modified by the vortex-dipole interaction, and this modulated interaction has either a ferromagnetic or a ferrimagnetic in nature.

IV. SCALING ANALYSIS

The excess susceptibility ($\Delta\chi_1^R(T)$) at low temperature (i.e. below T_{min}) exhibits an exponential temperature dependent behavior. Which is an indication of

some temperature dependent relaxation or opening of some kind of energy gap below T_{min} . The definition of $\Delta\chi_1^R(T)$ is shown by Eqn. 1. All these graphs can be scaled by a single universal equation (Eqn. 2). FIG. 6a shows the plot of $\Delta\chi_1^R(T)$ below T_{min} of B1, B2 and B3 composite,

$$\Delta\chi_1^R(T) = \delta\chi_1^R(T) - \delta\chi_1^R(T_{min}) \quad (1)$$

$$\Delta\chi_1^R(T) = A + b * \exp\left(-\frac{\Delta_0}{k_B T}\right) \quad (2)$$

where A, b and Δ_0 are constants. In FIG. 6b the scaled graph of $\Delta\chi_1^R(T)$ of the composites B1, B2, and B3 is displayed. Similarly $\Delta\chi_1^R(T)$ plot of B4, B5 and B6 are shown in FIG. 6c, and the corresponding scaled curves are shown in FIG. 6d. and FIG. 6d illustrate that the

TABLE III. PS- Particle size.

Material	Gd ₂ O ₃ ,(PS nm/ μ m)	h_{dc} (Oe)	$\Delta\chi_1^R$ (T) = A + b *exp(- $\frac{\Delta_0}{k_B T}$)		
			A	b	$\frac{\Delta_0}{k_B}$
B1-LCu(94)+GdO(6)	Bulk(μ m)	0 Oe	1.364	-1.487	0.69
B2-LCu(90)+GdO(10)	Bulk(μ m)	0 Oe	1.44	-1.61	1.09
B3-LCu(76)+GdO(24)	Bulk(μ m)	0 Oe	0.357	-0.410	0.98
B3-LCu(76)+GdO(24)	Bulk(μ m)	10 Oe	0.585	-0.68	0.89
B3-LCu(76)+GdO(24)	Bulk(μ m)	100 Oe	0.65	-0.76	0.83
B3-LCu(76)+GdO(24)	Bulk(μ m)	500 Oe	0.72	-0.83	0.69
B3-LCu(76)+GdO(24)	Bulk(μ m)	1000 Oe	0.78	-0.88	0.59
B4-LCu(90)+GdO600(10)	25(nm)	0 Oe	1.54	-1.67	0.46
B5-LCu(90)+GdO800(10)	45(nm)	0 Oe	4.07	-4.18	0.11
B6-LCu(90)+GdO950(10)	60(nm)	0 Oe	5.83	-5.90	0.038

nature of ES (or the change of the diamagnetic fraction) can be described by a single, universal equation or curve, regardless of the effective interface between LCu and GdO. The respective values of the corresponding parameters used in Eqn. 2 (i.e.A,b, Δ_0) of all the composites are given in Table II. FIG. 7 illustrates how the associated parameters vary as a function of particle size and the DC field. The change of $\frac{\Delta_0}{k_B}$, b and A against particle size of GdO is shown in FIG. 7a, FIG. 7b and FIG. 7c, respectively. Similarly, the variation of the corresponding parameters (i.e. $\frac{\Delta_0}{k_B}$, b and A) against dc field are shown in FIG. 7d,FIG. 7e and FIG. 7f, respectively.

The amplitude of $\frac{\Delta_0}{k_B}$ is observed to decrease with increasing the particle size of GdO, T_{min} also shows the similar behavior (Shown in the inset of FIG. 3a). The dc field dependent behaviour of $\frac{\Delta_0}{k_B}$ (shown in FIG. 7d) below 100 Oe is not so significant and above 100 Oe the decrement is very significant, which almost mimic the dc field dependent behavior of T_{min} .below 100 Oe is not so significant and above 100 Oe the decrement is very significant, which almost mimic the dc field dependent behavior of T_{min} . As previously stated, due to finite vortex motion, the strength of the vortex dipole interaction increases up to 100 Oe of the dc bias field and subsequently decreases above $h_{dc} > 100$ Oe. The dc field superimposed $|\chi_2|(T)$ measurement also shows an initial increase in ferromagnetic correlation at a lower dc bias field value ($h_{dc} < 100$ Oe), followed by a decrease in ferromagnetic (or ferrimagnetic) correlation at a larger dc field amplitude (i.e. $h_{dc} > 100$ Oe). Additionally, as evidenced by the vortex dipole interaction and ferromagnetic (or ferrimagnetic) type correlation, the dc field dependent behaviour of T_0 and T_{min} also exhibits similar behaviour.

The residue of all the fitted curve is shown in FIG. 8. The random ness of the residue across the zero point indicates the fitted equation used here is valid for the experimentally obtained graph. Therefore, Eqn.2 infer opening up of some type of energy gap much below the superconducting transition temperature and the second harmonic data indicates the presence of spontaneous magnetic moment in that particular energy state. Therefore, it can be

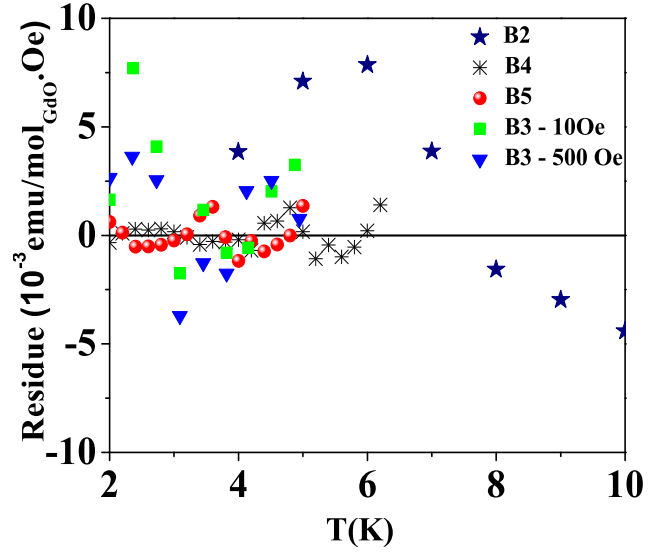


FIG. 8. (Colour Online)Residue of the fitted graph of B2, B4, B5, B3 at different magnetic field are shown.

inferred that the value of $\frac{\Delta_0}{k_B}$ and T_{min} is determined by the strength of the ferromagnetic or ferrimagnetic type of interaction between the Gd³⁺ spins via vortex. According to FIG. 7b, the parameter "b" decreases in a nonlinear manner as GdO particle size increases. however, it grows as the amplitude of the dc bias field grows (as illustrated in FIG. 7f). The sharpness of the ES is defined here by the parameter "b," which also denotes the reduction of the diamagnetic fraction. As shown in FIG. 7b and FIG. 7f, the sharpness of the ES reduces with decreasing effective interface and increases with rising amplitude of dc bias field. The parameter "A" increases as the GdO particle size increases (as shown in FIG. 7c), but it remains nearly same against the amplitude of the dc bias field (as seen in the inset of FIG. 7f). This parameter can be related to the disorder at the bulk of GdO because the disorder decreases with increasing GdO par-

ticle size, which causes its effective negative value to decrease. However, it remains constant with dc field for a specific material (in this case, B3) because the disorder cannot be tuned by a magnetic field, so it shows almost constant value against dc magnetic field. Another important point is the tunability of the energy barrier with the magnetic field. The energy value of these states are almost $\sim 10^{-6}$ eV much lower than the energy gap of the superconductor LCu (\sim meV) and also spin polarized in nature, which we believe can be a suitable candidate for the YSR state. By examining the residue plotted in FIG. 8, one may determine the correctness of the fitting.

It displays the difference between the real experimentally obtained graph and the fitted graph. Here, the fitting has been done by taking into account the initial parameter $\Delta_0 = k_B T_{min}$ ($k_B = 8.61 \times 10^{-5} \frac{eV}{K}$). The acquired values are then fed back into the equation a second time, iteratively fitting the graph.

A. CONCLUSION

Therefore, the excess susceptibility behavior at low temperatures and a finite value of $|\chi_2|(T)$ at zero bias dc

field around the same temperatures represent a modulated ferromagnetic or ferrimagnetic interaction between Gd^{+3} spins in GdO, with the modulation occurring as a result of vortex dipole interaction. The emergence of the spin triplet YSR state is indicated by this kind of activity. The Majorana zero mode is connected to the excitation of the YSR band, which is why the Majorana Fermion is being employed as a Q-bit in quantum computers. This is the essential significance of the YSR state. This work thus points to a route for discovering YSR type Q-bits utilising high T_C cuprate superconductors. Additional microscopic investigations, including as STM, STS, neutron scattering, etc., are necessary to demonstrate the existence of the spin triplet YSR state in these kinds of composite materials.

V. ACKNOWLEDGMENT

We thank Er. Kranti Kumar Sharma for fruitful discussions.

-
- [1] J. Bardeen, L. N. Cooper, J. R. Schrieffer, Phys. Rev. **108**, 1175 (1957).
- [2] S.Nadj-Perge et al., Science **346**, 602(2014).
- [3] Hiroyuki Shiba, Prog. Theor. Phys. **40**, 435 (1968).
- [4] S. Nadj-Perge et al., Phys. Rev. B **88**, 020407 (2013).
- [5] B. Braunecker and P. Simon, Phys. Rev. Lett. **111**, 147202 (2013).
- [6] A. I. Rusinov, JETP Lett. **9**, 85 (1969).
- [7] W. Bauriedl, Phys. Rev. Lett. **47**, 1163 (1981).
- [8] A.V. Balatsky et al., Rev. Mod. Phys. **78**, 373 (2006).
- [9] Gerbold C. Ménard et al., Nature Phys. **11**, 1013 (2015).
- [10] Shuai-Hua Ji et al., Phys. Rev. Lett. **100**, 226801 (2008).
- [11] D. K. Morr and J. Yoon, Phys. Rev. B **73**, 224511 (2006).
D. K. Morr and N. A. Stavropoulos, Phys. Rev. B **67**, 020502 (2003).
- [12] A. Yazdani et al., Science **275**, 1767 (1997).
- [13] M. Ruby et al., Phys. Rev. Lett. **117**, 186801 (2016).
M. Ruby et al., Phys. Rev. Lett. **120**, 156803 (2018).
- [14] D. J. Choi et al., Nat. Commun. **8**, 15175 (2017).
- [15] L. Schneider, npj Quantum Mater. **4**, 42 (2019).
- [16] N. Hatter et al., Nat. Commun. **6**, 8988 (2015).
- [17] L. Cornils, et al., Phys. Rev. Lett. **119**, 197002 (2017).
- [18] D. J. Choi, et al., Phys. Rev. Lett. **120**, 167001 (2018).
- [19] Shuai-Hua Ji et al., Phys. Rev. Lett. **100**, 226801 (2008).
- [20] P. Visani et al., Phys. Rev. Lett. **65**, 1514 (1990).
- [21] F. Bernd Muller-Allinger et al., Phys. Rev. Lett. **84**, 3161 (2000).
- [22] F. Bernd Muller-Allinger and Ana Celia Mota, Phys. Rev. B **62**, R6120 (2000).
- [23] Alban L. Fauchère et al., Phys. Rev. Lett. **82**, 3336 (1999).
- [24] Kazumi Maki and Stephan Haas, Phys. Lett. A. **272**, 271 (2000).
- [25] Roman M. Lutchyn et al., Phys. Rev. Lett. **105**, 077001 (2010).
- [26] Charles P. Bean, Rev. Mod. Phys. **36**, 31 (1964).
- [27] P.W. Anderson and Y.B. Kim, Rev. Mod. Phys. **36**, 39 (1964).
- [28] G. Ravi Kumar and P. Chaddah, Phys. Rev. B **39**, 4704 (1989).
- [29] K-H. Muller et al., Physica C **158**, 366 (1989).
- [30] S. Fujiki and S. Katsura, Prog. Theo. Phys., **65**, 1130 (1981).
- [31] K. Binder and A.P. Young, Rev. of Mod. Phys., **58**, 807 (1986).
- [32] T. Bitoh et al., J. Magn. Magn. Mater. **154**, 59 (1996).
- [33] A. Bajpai and A. Banerjee, Phys. Rev. B **55**, 12 439 (1997); A. Bajpai and A. Banerjee, Phys. Rev. B **62**, 8996 (2000); A. Bajpai and A. Banerjee, J. Phys. Condens. Matter **13**, 637 (2001).
- [34] Sunil Nair and A. Banerjee, Phys. Rev. Lett. **93**, 117204 (2004); A. K. Pramanik and A. Banerjee, Phys. Rev. B **82**, 094402 (2010).
- [35] S. Mukherjee and R. Ranganathan, Phys. Rev. B **54**, 9267 (1996); S. Mukherjee et al., Solid State Commun. **98**, 321 (1996); A. Chakravarti and R. Ranganathan, Solid State Commun. **82**, 591 (1992).
- [36] G. Sinha and A. Majumdar, J. Magn. Magn. Mater. **185**, 18 (1998).
- [37] Toshikazu Sato and Yoshihito Miyako, J. Phys. Soc. Jpn. **51**, 1394 (1982).
- [38] Sunil Nair and A. Banerjee, Phys. Rev. B **68**, 094408, (2003).
- [39] A. Chakravarti et al., Solid State Commun. **82**, 591 (1992).
- [40] D. Bhattacharya et al., Appl. Phys. Lett. **57**, 2145 (1990).
- [41] Biswajit Dutta et al., Rev. Sci. Instrum. **91**, 123905 (2020).
- [42] A. K. Pramanik and A. Banerjee, Phys. Rev. B **81**, 024431 (2010).
- [43] Biswajit Dutta et al., AIP Conference Proceedings **2115**, 030515 (2019). B Dutta and A Banerjee, Phys. Rev. B

- 106**, 134520 (2022).
- [44] R. M. Moon and W. C. Kochler, Phys. Rev. B, **11**, 1609 (1975).
- [45] B. Antic et al., Phys. Rev. B, **58**, 3212 (1998).
- [46] E. L. Correa et al., AIP Advances **6**, 056112 (2016).
- [47] V. Mourik et al., Science **336**, 1003 (2012).